LETTER TO THE EDITOR

Discovery and characterization of novel potent non-covalent small molecule inhibitors targeting papain-like protease from SARS-CoV-2

To the Editor:

The papain-like protease (PL^{pro}), as one of the most important proteases of SARS-CoV-2, has emerged as a highly promising target protein, its inhibitor probably holds dual potentials, namely blocking the cleavage of viral polyprotein and intercepting the deubiquitination and deISGylation functions to restore antiviral immunity[1]. However, the developing progress of PL^{pro} inhibitors has been relatively very slow[2,3], only one small molecule inhibitor, HL-21, was approved for its phase I study. Herein, we present our latest endeavors in the discovery of imidazo[4,5-*b*]pyridine derivatives as novel PL^{pro} inhibitors through structure-based drug design for hit compound **A0** from our previous high-throughput screening program[4] (Fig. 1A), in which 51 novel derivatives were synthesized (Fig. 1B). Multiple compounds exhibited excellent PL^{pro} inhibitory activities, especially six compounds' IC$_{50}$ values are below 100 nmol/L, which are 30−50 folds increasing compared to **A0**, and they also could dose-dependently inhibit the deubiquitination and deISGylation functions of PL^{pro}, restoring downstream IFN-β expression to enhance host antiviral innate immune responses. More importantly, the preferred compounds **39** and **45** also have potent inhibitory activities against the Delta and Omicron BA.5

variants of SARS-CoV-2. Besides, the binding mechanism was investigated by molecular docking, HDX-MS technique and residue mutation experiments, indicating these compounds are reversible non-covalent PL^{pro} inhibitors. Overall, this study has successfully identified a class of promising non-covalent small-molecule PL^{pro} inhibitors, which lay a robust foundation for discovering more effective therapeutic drug with a new scaffold for COVID-19.

1. The discovery of hit compound and rational design for novel PL^{pro} inhibitors

Considering the multidimensional biological functions of PL^{pro} that its inhibitors not only inhibit viral replication but also enhance host immunity[5], we early initiated a high-throughput screening (HTS) program and discovered compound **A0** has a good inhibition against PL^{pro} with IC$_{50}$ value of 2.71 ± 0.18 μmol/L (Fig. 1A)[4]. Through the molecular docking analysis, we found that the imidazo[4,5-*b*]pyridine scaffold of **A0** located at the S4 subsite of PL^{pro} forms a $\pi-\pi$ stack with the aromatic ring of Tyr268, the butanamide group of N^1-substituent forms two key hydrogen bond interactions with Asp164 and Gln269, and the *o*-tolyl group occupies the S3 subsite. The benzylthio segment extends into the BL2 groove, donating its hydrophobic interaction with PL^{pro} (Fig. 1B).

To obtain more potent PL^{pro} inhibitors, we conducted an in-depth structure−activity relationship (SAR) study. Firstly, the simple structural optimizations at the S3 or S4 subsite were launched to give compounds **1**−**9** (Fig. 1B). However, these modifications did not bring better inhibitory potencies than **A0**, probably due to the amide substitution being on the imidazole ring failing to induce a favorable conformation in the pocket of PL^{pro} (Supporting Information Table S1 and Fig. S1a−b).
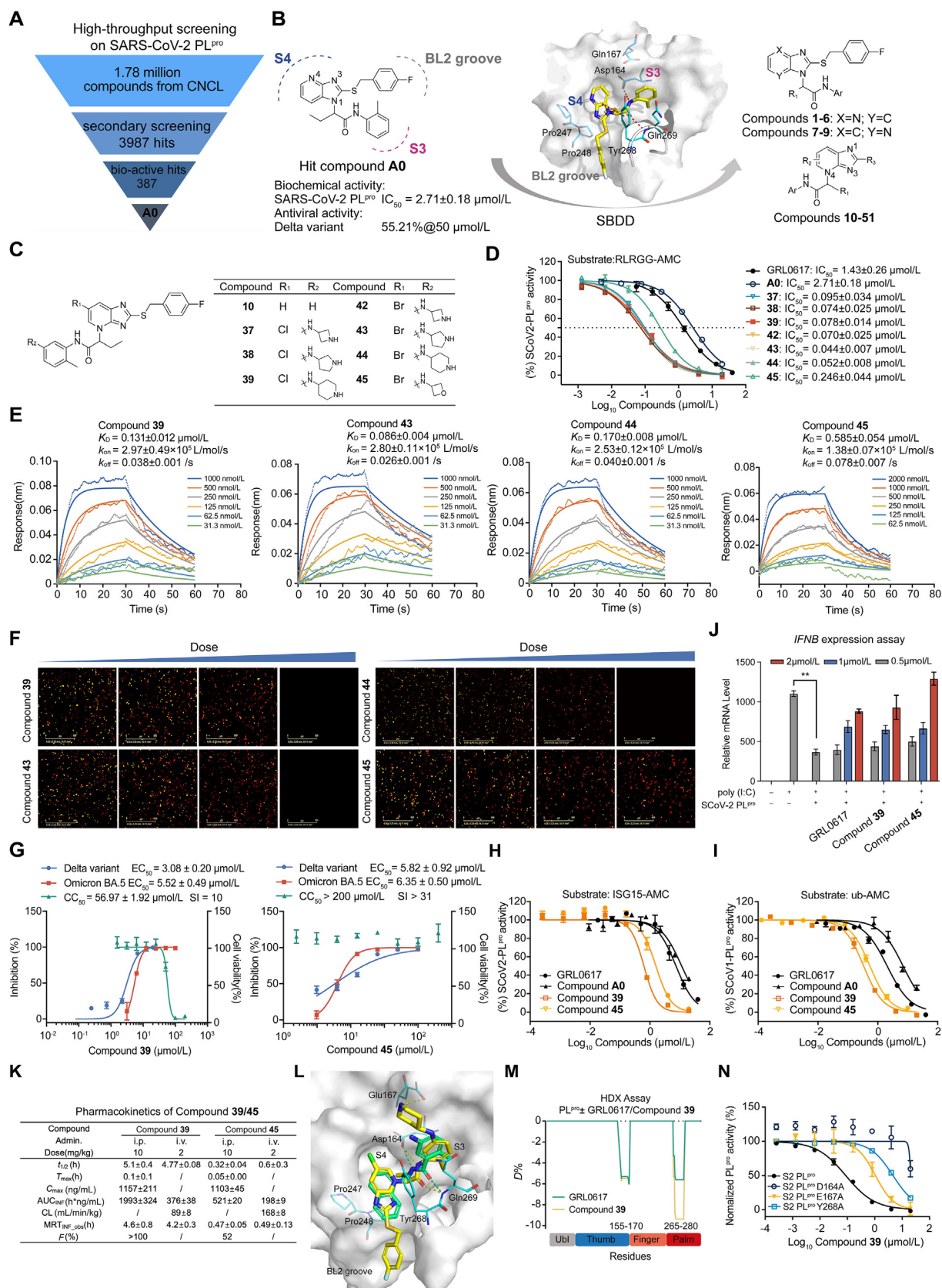

Figure 1   Discovery and characterization of potent novel non-covalent inhibitors targeting papain-like protease from SARS-CoV-2. (A) Flowchart the HTS and hit validation process of **A0**. (B) Rational design for the discovery of novel non-covalent SARS-CoV-2 PL^{pro} inhibitors (**A0**: yellow stick; interaction: red dashed lines; key residues: cyan lines; PDB: 7CJM). (C) and (D) *In vitro* inhibition for SARS-CoV-2 PL^{pro} of the GRL0617, **A0** and selected compounds. Data are presented as mean $\pm$ SD. (E) Kinetics characterization of these novel PL^{pro} inhibitors

Consequently, we moved the butanamide fragment from N^1-position to N^4-position for in-depth structural modifications to form compounds **10−27**. By analyzing the binding mode of active compound **10** with PL^{pro}, we observed no interaction between compound **10** and the key residue Glu167 (Fig. S1c), which however, it is a key residue for PL^{pro} and ubiquitin binding, forming the two hydrogen bond interactions with the Arg72 of ubiquitin (Supporting Information Fig. S2). Therefore, we introduced various heterocyclic substitutions on the o-tolyl moiety of compound **10** to create interactions with the key residue Glu167 and designed compounds **28−51** (Fig. 1B and C)[6]. Notably, 26 compounds exhibited stronger PL^{pro} inhibitory activities than **A0**, particularly, six compounds (**37−39** and **42−44**) demonstrated excellent PL^{pro} inhibitory activities with IC$_{50}$ values below 100 nmol/L, showing the most potent SARS-CoV-2 PL^{pro} inhibitory activities (Fig. 1C and D and Supporting Information Tables S1−S3). Furthermore, through chiral separation of compounds **39** and **45**, it was discovered that the (S)-configuration of both compounds exhibited significantly higher activity compared to their (R)-configuration (Supporting Information Tables S3, S4 and Figs. S3, S4). Meanwhile, they also significantly inhibited PL^{pro} of SARS-CoV-1 (Tables S1−S3). The synthetic steps of target compounds **1−51** are shown in Supporting Information Scheme S1. In addition, we also evaluated the selectivity against other coronavirus PL^{pro} and host proteases, the results display nearly no inhibition toward these proteases, which indicated these derivatives possess a high selectivity (Supporting Information Tables S5 and S6).

2. The biological activity evaluations for the representative compounds

To exclude the possibility of nonspecific inhibition and characterize enzyme inhibition kinetics, we first measured kinetic constants including the affinity constant (K_D), association rate constant (k_{on}) and dissociation rate constant (k_{off}) using bio-layer interferometry BLI analysis for nineteen compounds including **A0**, **10**, **28−30**, **32−34** and **37−47** based on their enzyme inhibition activities and

structural diversity (Fig. 1E and Supporting Information Fig. S5 and Table S7). The correlation analysis showed good correlation between K_D and IC$_{50}$ of most compounds ($R^2 = 0.69$, $P < 0.0001$) (Supporting Information Fig. S6). Specially, six compounds **37−39** and **42−44**, with the best SARS-CoV-2 PL^{pro} inhibition activities (IC$_{50} < 100$ nmol/L), demonstrated excellent kinetic features, such as strong binding affinities ($K_D < 0.18$ μmol/L) and very slow dissociation behaviors ($k_{off} < 0.08$ /s), indicating about 20-fold improvement in binding affinity compared to **A0** and GRL0617, the slow dissociation behaviors suggested these compounds may have better cellular and in vivo efficacy. Taken together, these data suggest that these compounds have favorable kinetic characteristics, and are reversible non-covalent small molecule PL^{pro} inhibitors.

To validate cellular PL^{pro} inhibition activity, we built a cell-based FlipGFP-PL^{pro} assay procedure[7,8] to assess the potential cellular activities for aforementioned compounds, in which compounds **39** and **43−45** demonstrated the most desirable antiviral activities with EC$_{50}$ of 2.41 ± 0.12 μmol/L (**39**), 2.33 ± 0.33 μmol/L (**43**), 3.81 ± 0.59 μmol/L (**44**) and 3.13 ± 0.75 μmol/L (**45**), representing at least a 4-fold improvement comparing with **A0** and GRL0617 (Fig. 1F and Supporting Information Fig. S7). Overall, these findings indicated that these compounds could potently suppress the PL^{pro} in cellular assay and provided evidence of membrane permeability and cellular protection for potential antiviral activities.

Subsequently, compounds **39**, **45** and GRL0617 were selected as the representative compounds to elucidate the antiviral activities in Vero E6 cell based on their inhibition activities and structural diversity. The results indicated that compounds **39** and **45** showed effective inhibitory effects on SARS-CoV-2 variant strains, displaying remarkably improved potencies against the Delta variant with EC$_{50}$ values of 3.08 ± 0.20 and 5.82 ± 0.92 μmol/L, respectively, which were nearly a 13-fold better than GRL0617 (EC$_{50} = 41.17 \pm 4.48$ μmol/L). For the Omicron BA.5 variant, compounds **39** and **45** showed EC$_{50}$ values of 5.52 ± 0.49 and 6.35 ± 0.50 μmol/L, respectively, representing almost a 6-fold improvement than GRL0617 (EC$_{50} = 33.32 \pm 10.16$ μmol/L) (Fig. 1G and Supporting Information Fig. S8). More importantly,

binding with the SARS-CoV-2 PL^{pro} through BLI analyses. BLI analysis shows the representative binding and disassociation curves of representative PL^{pro} inhibitors to PL^{pro}, The K_D, k_{on} and k_{off} value displayed for each sample is the mean value of three independent measurements. Data are presented as mean $\pm$ SEM. (F) Profiling of novel PL^{pro} inhibitors in the cell-based FlipGFP-PL^{pro} assay. Fluorescence images of representative PL^{pro} inhibitors (20, 5, 1.25, 0.32 μmol/L) from the FlipGFP-PL^{pro} assay. Scale bar, 800 μm. (G) Antiviral activity in Vero E6 cell against SARS-CoV-2 Delta variant and Omicron BA.5 variant. Inhibition rates of **39** and **45** on Vero E6 cells infected with SARS-CoV-2 Delta variant (blue), Omicron BA.5 variant (red) with an MOI of 0.01, viral copies were determined by qRT-PCR after 24 h post-infection, dose−response curves of the indicated antivirals in the plaque-reduction assay (EC$_{50}$) and corresponding cytotoxicity (CC$_{50}$) to Vero E6 cells were measured by CCK-8 assays. (H) and (I) In vitro PL^{pro} inhibition assay, cleavage of Ub-AMC by SARS-CoV-1 PL^{pro} and cleavage of ISG15-AMC by SARS-CoV-2 PL^{pro} in the presence of different concentrations of inhibitors were measured and normalized to DMSO control, dose−response curves are presented. Data are presented as mean $\pm$ SEM ($n = 3$, biological replicates). (J) qPCR assay, effect of compounds on SARS-CoV-2 PL^{pro} mediated *IFNB* expression level. HeLa cells were transfected with PL^{pro} and treated with poly(I:C) for 12 h, following a 3 h pretreatment with compounds at indicated concentrations. *IFNB* mRNA expression was analyzed by qPCR. Data are presented as mean $\pm$ SD, P values were calculated using t-test, **$P < 0.01$. (K) PK parameters of **39** and **45** in ICR mice. (L) The superposition of binding modes of compound **39** and GRL0617 with PL^{pro} (**39**: yellow stick; GRL0617: green stick; interaction: yellow dashed lines for **39**, green dashed lines for GRL0617; key residues: cyan lines; PDB 7LBS). (M) Comparative HDX-MS studies of PL^{pro} upon compound **39** and GRL0617 interactions. A negative value in the y axis (D, %) represents protection (stabilization) against deuterium exchange in the corresponding region of the receptor depicted in the x axis when a binding event takes place. (N) Effects of binding-site mutations on the activation of PL^{pro} after treatment with inhibitors, determined with PL^{pro} inhibition assays.

their CC_{50} values are more than 50 µmol/L, indicating they have good safety profiles (SI > 10).

Given the deubiquitination and deISGylation activities of PL^{pro} that could affect downstream type I interferon response, we tested whether these compounds could inhibit the deubiquitination and deISGylation activities of PL^{pro}. The results showed that they all could dose-dependently inhibit the deubiquitination activities of both SARS-CoV-1 and SARS-CoV-2 PL^{pro}, and deISGylation activities of SARS-CoV-2 PL^{pro} (Fig. 1H and I and Supporting Information Table S8). Moreover, compounds **39** and **45** could fully restore *IFNB* expression at 2 µmol/L (Fig. 1J), potentially enhancing the host's antiviral innate immune response.

In view of the potent inhibitory activities against PL^{pro} and antiviral activities *in vitro*, compounds **39** and **45** were selected to evaluate their pharmacokinetics (PK) profiles in ICR mice. Compound **39** exhibited better pharmacokinetic profiles, such as longer half-life ($t_{1/2}$), better maximum concentration (C_{max}), higher plasma exposure with the area under the curve (AUC) and smaller clearance rate (CL) than compound **45** (Fig. 1K). These PK results were also consistent with the stability results of the two compounds in mouse liver microsomes (Supporting Information Table S9), indicating compound **39** has more desirable druggability.

3. Binding mechanism exploration of preferred compounds with SARS-CoV-2 PL^{pro}

To elucidate the molecular interactions between the compounds and SARS-CoV-2 PL^{pro}, we further analyzed the superposition of binding modes of preferred compound **39** and GRL0617 with PL^{pro}. It was discovered that the binding conformation of **39** was similar to that of GRL0617 with PL^{pro} by molecular docking (Fig. 1L). The main difference, compared to GRL0617, was that the benzylthio group of **39** could extend into the BL2 groove, forming hydrophobic interactions.

To further validate the binding sites of the inhibitors, hydrogen/deuterium exchange coupled with mass spectrometry (HDX-MS) techniques was performed (Fig. 1M and Supporting Information Fig. S9). In comparison to GRL0617, compound **39** showed a tighter binding to both the residues 155−170 and 265−280 regions (including the BL2 groove) of the pocket, providing evidence for the interaction of compound **39** with the BL2 groove. This finding verified the docking analysis results and explained why compound **39** exhibited superior inhibitory effects compared to GRL0617. Furthermore, in order to validate this result, we have launched the residue mutation experiments, and the results showed that mutations of Asp164, Glu167 and Tyr268 to alanine (D164A/E167A/Y268A) led to the loss or significant reduction of activity, indicating that these compounds formed critical interactions with residues Asp164, Glu167 and Tyr268 (Fig. 1N, Supporting Information Fig. S10 and Table S10). Overall, the HDX-MS and mutation experiments further validated the docking results, indicating that these inhibitors interacted with key residues of PL^{pro}, including Asp164, Glu167, Pro247, Pro248, Tyr268 and Gln269, thereby occupying the channel for substrates to reach the catalytic site of PL^{pro} and exerting inhibitory effects.

In conclusion, we performed a SAR study by SBDD and scaffold hopping strategies to design and synthesize 51 novel derivatives, in which 26 compounds exhibited stronger PL^{pro} inhibitory activities than hit compound **A0**. Particularly, six compounds (**37−39** and **42−44**) demonstrated excellent PL^{pro} inhibitory activities with IC_{50} values below 100 nmol/L,

approximately 30−50 folds improvement compared to the **A0**, already becoming one of the strongest effective PL^{pro} inhibitors until now. Meanwhile, these compounds could also dose-dependently inhibit the deubiquitination and deISGylation of PL^{pro}, hopefully restoring downstream IFN-β expression and enhancing host antiviral innate immune responses. Besides, the determination of kinetic parameters by BLI analysis, molecular docking, HDX-MS and residue mutation assay were performed separately to validate the binding mechanism of these compounds, all results supported the fact that these compounds are reversible non-covalent small molecule PL^{pro} inhibitors. More importantly, compounds **39** and **45** could potently inhibit the Delta and Omicron BA.5 variants of SARS-CoV-2, and compound **39** exhibited better PK properties than compound **45** and was more suitable for further explorations. Taken together, this investigation identified a series of potent novel non-covalent small molecule inhibitors that possess good kinetic characteristics, significant antiviral activities and PK profiles, which might serve as a more favorable drug candidate for further optimization to discover more effective PL^{pro}-targeted therapeutic agents.

Author contributions

Yu Zhou, Jia Li, Leike Zhang, Jie Zheng, Linxiang Zhao and Hong Liu conceived and designed this project. Miao Zheng, Bo Feng, Yumin Zhang, Xin Liu, Yi Zang and Yu Zhou wrote the manuscript. Miao Zheng, Bo Feng, Yumin Zhang and Xin Liu analyzed the data and drew figures and tables. Miao Zheng, Na Zhao, Zichao Xu, Zhiyan Qu and Zhidong Jiang synthesized the target compounds and key intermediates. Bo Feng, Hui Liu and Shizhao Chen performed *in vitro* and *in vivo* experiments on PL^{pro} inhibition. Leike Zhang and Yumin Zhang designed and performed antiviral assays. Xin Liu performed *IFNB* expression assay and HDX-MS experiments. Xinheng He and Xi Cheng calculated ECD spectra. Miao Zheng conducted molecular docking. All authors have approved the final version of the manuscript.

Conflicts of interest

The authors declare no conflict of interest.

Appendix A. Supporting information

Supporting information to this article can be found online at https://doi.org/10.1016/j.apsb.2024.04.011.

References

1. Yang HT, Rao ZH. Structural biology of SARS-CoV-2 and implications for therapeutic development. *Nat Rev Microbiol* 2021;**19**:685−700.

3290   Miao Zheng et al.

2. Li G, Hilgenfeld R, Whitley R, De Clercq E. Therapeutic strategies for COVID-19: progress and lessons learned. *Nat Rev Drug Discov* 2023; **22**:449−75.
3. Tan H, Hu Y, Jadhav P, Tan B, Wang J. Progress and challenges in targeting the SARS-CoV-2 papain-like protease. *J Med Chem* 2022;**65**: 7561−80.
4. Zang Y, Su M, Wang Q, Cheng X, Zhang W, Zhao Y, et al. High-throughput screening of SARS-CoV-2 main and papain-like protease inhibitors. *Protein Cell* 2023;**14**:17−27.
5. Shin D, Mukherjee R, Grewe D, Bojkova D, Baek K, Bhattacharya A, et al. Papain-like protease regulates SARS-CoV-2 viral spread and innate immunity. *Nature* 2020;**587**:657−62.
6. Shen Z, Ratia K, Cooper L, Kong D, Lee H, Kwon Y, et al. Design of SARS-CoV-2 PLpro inhibitors for COVID-19 antiviral therapy leveraging binding cooperativity. *J Med Chem* 2022;**65**:2940−55.
7. Ma C, Sacco MD, Xia Z, Lambrinidis G, Townsend JA, Hu Y, et al. Discovery of SARS-CoV-2 papain-like protease inhibitors through a combination of high-throughput screening and a FlipGFP-based reporter assay. *ACS Cent Sci* 2021;**7**:1245−60.
8. Ma C, Xia Z, Sacco MD, Hu Y, Townsend JA, Meng X, et al. Discovery of di- and trihaloacetamides as covalent SARS-CoV-2 main protease inhibitors with high target specificity. *J Am Chem Soc* 2021;**143**: 20697−709.

Miao Zheng[a,c,†], Bo Feng[b,d,†], Yumin Zhang[e,†], Xin Liu[c,†], Na Zhao[a,c], Hui Liu[d], Zichao Xu[c], Xinheng He[c], Zhiyan Qu[c], Shizhao Chen[d], Zhidong Jiang[c,f], Xi Cheng[c], Hong Liu[c], Yi Zang[f], Linxiang Zhao[a,*], Jie Zheng[c,*], Leike Zhang[e,h,*], Jia Li[b,d,g,*], Yu Zhou[a,c,g,*]

[a]*Key Laboratory of Structure-Based Drugs Design & Discovery of Ministry of Education, Shenyang Pharmaceutical University, Shenyang 110016, China*
[b]*School of Life Sciences and Biopharmaceuticals, Shenyang Pharmaceutical University, Shenyang 110016, China*
[c]*Shanghai Institute of Materia Medica, Chinese Academy of Sciences, Shanghai 201203, and University of Chinese Academy of Sciences, Beijing 100049, China*
[d]*State Key Laboratory of Chemical Biology, Shanghai Institute of Materia Medica, Chinese Academy of Sciences, Shanghai 201203, and University of Chinese Academy of Sciences, Beijing 100049, China*
[e]*State Key Laboratory of Virology, Wuhan Institute of Virology, Center for Biosafety Mega-Science, Chinese Academy of Sciences, Wuhan 430071, China*
[f]*Lingang Laboratory, Shanghai 200031, China*
[g]*School of Pharmaceutical Science and Technology, Hangzhou Institute for Advanced Study, University of Chinese Academy of Sciences, Hangzhou 310024, China*
[h]*Hubei Jiangxia Laboratory, Wuhan 430200, China*

*Corresponding authors.
E-mail addresses:* linxiang.zhao@vip.sina.com (Linxiang Zhao), jzheng@simm.ac.cn (Jie Zheng), zhangleike@wh.iov.cn (Leike Zhang), jli@simm.ac.cn (Jia Li), zhouyu@simm.ac.cn (Yu Zhou)

[†]These authors made equal contributions to this work.